pp 271–295. © Royal Aeronautical Society 2019
doi:10.1017/aer.2019.123

Parameter estimation of aircraft using extreme learning machine and Gauss-Newton algorithm

H. O. Verma and N. K. Peyada
homverma@aero.iitkgp.ernet.in; homverma@gmail.com;
nkpeyada@aero.iitkgp.ac.in
Department of Aerospace Engineering
Indian Institute of Technology Kharagpur
India

ABSTRACT

The research paper addresses the problem of estimating aerodynamic parameters using a Gauss-Newton-based optimisation method. The process of the optimisation method lies on the principle of minimising the residual error between the measured and simulated responses of the system. Usually, the simulated response is obtained by integrating the dynamic equations of the system, which is found to be susceptible to the initial values, and the integration method. With the advent of the feedforward neural network, the data-driven regression methods have been widely used for identification of the system. Among them, a variant of feedforward neural network, extreme learning machine, which has proven the performance in terms of computational cost, generalisation, and so forth, has been addressed to predict the responses in the present study. The real flight data of longitudinal and lateral-directional motion have been considered to estimate their respective aerodynamic parameters. Furthermore, the estimates have been validated with the values of the classical estimation methods, such as the equation-error and filter-error methods. The sample standard deviations of the estimates demonstrate the effectiveness of the proposed method. Lastly, the proof-of-match exercise has been conducted with the other set of flight data to validate the estimated parameters.

Keywords: Non-linear modelling; Extreme Learning Machine Network; Gauss-Newton Method; Parameter Estimation

NOMENCLATURE

a_x, a_y, a_z	Linear accelerations of aircraft along x, y and z axes (m/s^2), respectively.
b	Wingspan (m).
$\bar{c}$	Mean aerodynamic chord of wing (m).
C_D, C_L, C_Y	Coefficients of drag, lift and side force, respectively.
C_l, C_m, C_n	Coefficients of rolling, pitching and yawing moment, respectively.
p, q, r	Angular rates: roll, pitch and yaw (rad/s), respectively.
V	True velocity of aircraft (m/s).

Received 20 February 2019; revised 21 August 2019; accepted 4 September 2019.

$\bar{V}$, $\bar{H}$, $\bar{W}$	Input weight matrix including bias, hidden layer output vector and output weight matrix, respectively.
$x_{i,\min}$, $x_{i,\max}$	Minimum and maximum value of the i^{th} input variable, respectively.
X, Y, Z	Input, predicted output and measured output, respectively.
$\bar{x}_{i,\min}$, $\bar{x}_{i,\max}$	Lower and upper limits of the i^{th} normalised input variable, respectively.
$\bar{x}$, $\bar{y}$, $\bar{z}$	Normalised input, predicted output and measured output, respectively.

Greek Notation

α	Angle-of-attack (rad).
β	Side-slip angle (rad).
ϕ, θ, ψ	Roll, pitch and yaw angle (rad), respectively.
δ_e, δ_a, δ_r	Elevator, aileron and rudder deflection (rad), respectively.

Abbreviations

ANFIS	Adaptive neuro-fuzzy inference system
ATTAS	Advanced technology testing aircraft system
EEM	Equation error method
ELM	Extreme learning machine
FEM	Filter error method
FFNN	Feedforward neural network
GN	Gauss-Newton
HLN	Hidden layer neuron
MSE	Mean square error
NV	Nominal value
OEM	Output error method
RBFNN	Radial basis function neural network
RFD	Real flight data
RNN	Recurrent neural network

1.0 INTRODUCTION

The determination of the aerodynamic forces and moments of an aircraft is a field of great interest and is more often accomplished by using the analytical and computational approaches. The analytical, computational fluid dynamic methods and wind-tunnel testing provide preliminary information about the aerodynamic parameters in the design phase, while they pose limitations due to the assumptions made about them, computational cost, scaling of the model and model wind-tunnel interference. The computation of the aerodynamic parameters from flight test data is a complementary step to understand the stability and control derivatives with more accuracy.

The aerodynamic forces and moments are often depicted in the form of a functional relationship with the linear and angular motion variables and control surface deflections, thus constituting an aerodynamic model[1,2]. The unknown parameters of the postulated aerodynamic model are extracted by minimising the error between the measured and simulated responses. Also, the widely used estimator based on the maximum likelihood function is applied to estimate the aerodynamic parameters through a deterministic analysis[3]. Such an

https://doi.org/10.1017/aer.2019.123 Published online by Cambridge University Press

estimator is categorised based on the stochastic noise treatment of the flight data as the output error method (OEM), equation error method (EEM) and filter error method (FEM)[4–6]. OEM and EEM can account for measurement and process noise, respectively, whereas FEM can account for both of them[7]. The estimation approaches based on the combination of state and parameters were also investigated to improve the quality of estimates through the stochastic analysis[8].

Over the past few decades, an alternative model building using feedforward neural network (FFNN) has gotten more attention from the researchers due to the advancement in the instrumentation and measurement units, which have enhanced the qualitative acquisition of the database from the cause-effect observations of the system. FFNN is capable of approximating the system behaviour using the measured database by providing training to the network parameters[9]. The training of the conventional FFNN needs a priori information of the network size, initial weights and biases, number of hidden layer neurons (HLNs) and their activation functions, number of epochs, and training algorithms such as steepest descent, Levenberg-Marquardt, scaled conjugate gradient, etc.[10–12] An early investigation of FFNN in the field of parameter estimation was found where the aerodynamic forces and moments were non-linearly mapped with the dependent motion and control variables of the aircraft[13]. Later, the investigation was carried out by applying the numerical analysis on the dataset of the trained FFNN, and the estimation techniques were named as Delta, Zero and Modified Delta methods[14,15]. The partial differentiation of the aerodynamic forces and moments concerning the motion and control variables were also implemented as a part of the gradient-based training algorithm of a multilayer FFNN to compute the corresponding aerodynamic parameters[16,17]. A non-linear least-square-based optimisation methodology was also investigated in the field of parameter estimation,[18] and the parameters of a flight manoeuvre at a high angle-of-attack regime were computed[19,20]. Variants of FFNN such as radial basis function neural network (RBFNN), recurrent neural network (RNN) and adaptive neuro-fuzzy inference system (ANFIS) were also applied in the non-linear mapping of the aerodynamic forces and moments to estimate the aerodynamic stability and control derivatives[21–24]. It is evident from the investigation carried out using the conventional FFNN and its variants mentioned above that the training of FFNN is a cumbersome task due to the number of epochs, slow convergence of learning strategies and trapping of the error function in local minima. The improper tuning of the initial parameters may either deteriorate the generalisation or increase the computational burden. Hence, to overcome the issues of conventional FFNN, its variant named extreme learning machine (ELM) was suggested by Huang et al.[25,26]. The ELM network consists of a single hidden layer that can be tuned analytically; hence, the computational cost is reduced significantly. The ELM network is found to be more generalised and robust in comparison to the conventional FFNN. The real-world problems of different fields such as forecasting, pattern recognition and classification have been solved using the ELM features[27–31].

The research paper utilises the ELM features in the non-linear modelling of the aircraft's dynamic model in a restricted sense for the application of aerodynamic parameter estimation. The quality assessment of the network has been carried out based on the statistical metric R^2 and mean square error (MSE). Furthermore, a non-linear optimisation based on the Gauss-Newton (GN) method has been applied to extract the longitudinal and lateral-directional aerodynamic parameters from the real flight data of research aircraft – namely, Hansa-3 and advanced technology testing aircraft system (ATTAS), respectively. The validation of the estimates using the proposed methodology has been carried out by comparison of the values and their respective standard deviations with those of the conventional parameter estimation

https://doi.org/10.1017/aer.2019.123 Published online by Cambridge University Press

methods and using the proof-of-match exercise. The research paper is organised as follows: the next section addresses the procedure of non-linear mapping using the ELM network, and the subsequent sections present the procedure of parameter estimation methodology, results and discussion and conclusion.

2.0 EXTREME LEARNING MACHINE BASED NEURAL MODELLING

The emergent of FFNN in the approximation of a system with lesser knowledge about the underlying physics has changed the view of computation in terms of accuracy and the computational cost. The supervised learning is widely used in the analysis as well as the operation of such a system. In our research work, a time series neural model of flight dynamics has been studied with FFNN in a restricted sense to estimate the aerodynamic parameters. The aircraft's motion is primarily governed by the aerodynamic forces and moments and defined by its states such as angle-of-attack, side-slip angle, attitude angles, true velocity, angular rates, linear accelerations, altitude, etc.[32,36] Using the measured motion and control variables, a time series neural model for longitudinal and lateral-directional motion[18] is established by neglecting the cross-coupling effects as shown in Fig. 1.

In the present research, only the previous data dependency of the desired response is presented with an assumption that the $(i+1)^{th}$ instant output variables are affected by the i^{th} instant input variables. Let us assume a conventional FFNN[11,12] of multi-input multi-output structure with the input and output variables of dimension $X \in R^{n_x}$ and $Z \in R^{n_y}$, respectively, and the hidden layer neurons of $H \in R^{n_h}$ as shown in Fig. 1. The input and output vectors for the training of the network can be expressed as follows:

$$\text{Input vector,} \qquad X(i) = \left[x_1(i),\ x_2(i),\ \ldots x_{n_x}(i)\right] \tag{1}$$

$$\text{Output vector,} \qquad Z(i+1) = [z_1(i+1),\ z_2(i+1),\ \ldots, z_{n_y}(i+1)] \tag{2}$$

As the quantities used for the non-linear mapping of the network differ in magnitude levels as well as physical significance, their normalisation has been performed to enhance the learning so that it is more effective by scaling the training data samples in a suitable range of $(\bar{x}_{max},\ \bar{x}_{\min})$[33]. The normalisation process of the input and output variables can be carried out as follows:

$$\bar{x}_i = \bar{x}_{i,\min} + \frac{(\bar{x}_{i,\max} - \bar{x}_{i,\min})}{(x_{i,\max} - x_{i,\min})}(x_i - x_{i,\min}) \tag{3}$$

The processing of the data takes place from the input layer neurons to the hidden layer neurons through the connecting weight $\bar{V}$ of dimension $n_{x+1} \times n_h$. As the hidden layer neurons use an activation function to introduce the non-linearity and the biases, the output of the hidden layer at the j^{th} neuron can be expressed as follows:

$$\bar{h}_j = g\left(\sum_{i=1}^{n_x} \bar{x}_i \bar{v}_{ij} + \bar{v}_{(n_x+1)j}\right), \tag{4}$$

where $\bar{v}_{ij}$, the element of $\bar{V}$, denotes the connecting weight between the i^{th} and j^{th} neurons of the input and the hidden layer, respectively. $\bar{v}_{(n_x+1)j}$ represents the bias of the j^{th} hidden layer

https://doi.org/10.1017/aer.2019.123 Published online by Cambridge University Press

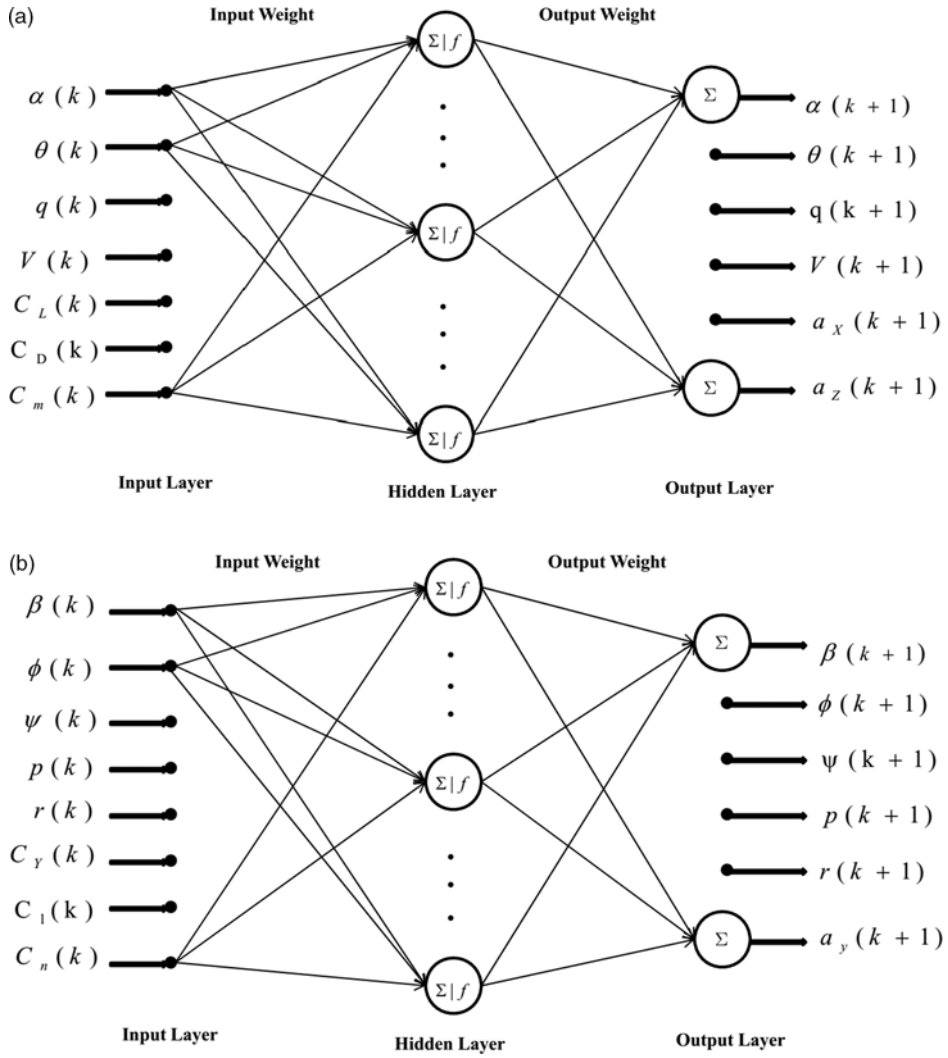

Figure 1. Structure of the neural model for parameter estimation.

neuron. $g(\cdot)$ denotes the functional relationship of the activation function for processing of the data.

The output of the network can be approximated using the connecting weights $\bar{W}$ as follows:

$$\bar{y}_k = \sum_{j=1}^{n_h} \bar{h}_j \bar{w}_{jk}, \tag{5}$$

where $\bar{h}_j$ is the element of the hidden layer output vector $\bar{H}$, and $\bar{w}_{jk}$, the element of the output weight $\bar{W}$, denotes the connecting weight between the j^{th} and k^{th} neurons of the hidden and the output layer, respectively.

Equations (1) – (5) represent the steps to be followed for processing of the data through the ELM network. Huang et al.[25,26] have investigated the single hidden layer FFNN for training as well as testing analytically and has proven the network's optimality and convergence.

https://doi.org/10.1017/aer.2019.123 Published online by Cambridge University Press

The input weights and biases of the hidden layer neurons are chosen randomly from a normal distribution, and the number of hidden layer neurons is determined based on the minimisation of the residual error between the measured and estimated responses as follows:

$$\sum_{i=1}^{N} \| Y(i) - Z(i) \| < \varepsilon, \tag{6}$$

where ε is the residual error, and N is the number of the data samples. ε is a significant value for a number of the hidden layer neurons lesser than the number of data samples.

The Equation (6) can also be expressed as follows:

$$\underset{\bar{W}}{min} \left\| \bar{H}\bar{W} - \bar{Z} \right\| \tag{7}$$

The objective is to minimise the output weight $\bar{W}$ of the equation, which is a set of linear equations. These equations are minimised using the least-square principle for $\bar{W}$. The output weight can be estimated as follows:

$$\hat{\bar{W}} = \bar{H}^* \bar{Z}, \tag{8}$$

where $\bar{H}^* = \left(\bar{H}^T \bar{H}\right)^{-1} \bar{H}^T$ is a minimum of all possible solutions obtained from the least-square and known as the Moore-Penrose inverse matrix. The equation is determined analytically for the assigned number of the hidden layer neurons and the corresponding activation function.

The accuracy of the neural model is expressed by the MSE as follows:

$$MSE = \frac{1}{N} \sum_{i=1}^{N} \sum_{k}^{n_y} (y_{ki} - z_{ki})^2 \tag{9}$$

A statistical quantity, which is the coefficient of determination (R^2) is defined to quantify the neural model for the prediction of the future outcomes based on the other related input dataset and is expressed as follows[35]:

$$R^2 = \frac{\sum_{i=1}^{N} (Z_i - Z_{avg.})^2 - \sum_{i=1}^{N} (Z_i - Y_i)^2}{n_y \sum_{i=1}^{N} (Z_i - Z_{avg.})^2}, \tag{10}$$

where $Z_{avg.}$ is the average value of the data samples of the measured output vector Z.

3.0 PARAMETER ESTIMATION METHODOLOGY

The current section demonstrates the optimisation methodology to extract the stability and control derivatives of an aerodynamic model. The neural models discussed in the previous section are used for the purpose of predictions with the different input samples. Among the input variables, the coefficients of aerodynamic forces and moments of a postulated aerodynamic model are obtained analytically and propagated through the network. The derivatives of the aerodynamic model, which are to be optimised, can be represented altogether as Θ.

https://doi.org/10.1017/aer.2019.123 Published online by Cambridge University Press

Therefore, the prediction of the observations at the $(i+1)^{th}$ instant through the neural model can be expressed as follows:

$$Y(i+1) = f(X(i), \bar{V}, \bar{W}, \Theta), \tag{11}$$

where $Y(i+1) = [y_1(i+1),\ y_2(i+1),\ \ldots, y_{n_y}(i+1)]$ and $f(\cdot)$ denotes the non-linear mapping through ELM network.

In the optimisation process, the cost function J, based on the likelihood function, is expressed to be minimised for Θ and R as follows[5]:

$$J(\Theta, R) = \frac{1}{2}\sum_{i=1}^{N} E_i^T R^{-1} E_i + \frac{N}{2}\ln\det(R) + \frac{n_y N}{2}\ln 2\pi, \tag{12}$$

where $E_i = [Z(i) - Y(i)]$ is the residual error, n_y is the number of output variables (observations) and R is the measurement noise covariance matrix.

In the present work, we have assumed that an aerodynamic model with their initial guess values, number of observations through the ELM network and the number of data samples are known before initiating the optimisation process. So, by taking the partial derivative of $J(\Theta, R)$ with respect to R and equating to zero, the Equation (12) turns out to the following expression:

$$R = \frac{1}{N}\sum_{i=1}^{N} E_i E_i^T \tag{13}$$

Therefore, the cost function is rewritten as follows:

$$J(\Theta) = \frac{1}{2} n_y N + \frac{N}{2}\ln\det(R) + \frac{n_y N}{2}\ln 2\pi \tag{14}$$

By neglecting the constant terms and without affecting the minimum value of the equation, the cost function can be expressed as follows:

$$J(\Theta) = \det(R) \tag{15}$$

The above cost function is minimised for the parameter Θ according to the GN method as follows:

$$\left(\frac{\partial J}{\partial \Theta}\right)_k = 0 \tag{16}$$

The subscript 'k' signifies about the k^{th} iteration of the optimisation process. Now, $\left(\partial J / \partial \Theta\right)_k$ can be approximated using Taylor's series expansion theory for the first two terms as follows:

$$\left(\frac{\partial J}{\partial \Theta}\right)_{k+1} \approx \left(\frac{\partial J}{\partial \Theta}\right)_k + \left(\frac{\partial^2 J}{\partial \Theta^2}\right)_k \Delta\Theta \tag{17}$$

https://doi.org/10.1017/aer.2019.123 Published online by Cambridge University Press

As $\partial J/\partial \Theta_{k+1} = 0$, therefore, the parameter update vector $\Delta\Theta$ can be expressed as follows:

$$\Delta\Theta = -\left[\left(\frac{\partial^2 J}{\partial \Theta^2}\right)_k\right]^{-1}\left(\frac{\partial J}{\partial \Theta}\right)_k, \tag{18}$$

where $\left(\frac{\partial J}{\partial \Theta}\right)_k = -\sum_{i=1}^{N}\left[\frac{\partial Y(i)}{\partial \Theta}\right]^T R^{-1}E_i$ and $\left(\frac{\partial^2 J}{\partial \Theta^2}\right)_k = \sum_{i=1}^{N}\left[\frac{\partial Y(i)}{\partial \Theta}\right]^T R^{-1}\left[\frac{\partial Y(i)}{\partial \Theta}\right]$ are defined at the k^{th} iteration of the optimisation process and are known as the gradient vector and Hessian matrix, respectively.

The forward difference approximation can be used to compute the response gradient matrix, $\left(\partial Y(i)/\partial \Theta\right)_{ij}$, as follows:

$$\left(\frac{\partial Y(i)}{\partial \Theta}\right)_{ij} \approx \frac{f(X(i-1), \bar{V}, \bar{W}, \Theta + \delta\Theta_j) - f(X(i-1), \bar{V}, \bar{W}, \Theta)}{\delta\Theta_j}, \tag{19}$$

where $i = 1, 2, 3 \ldots, N$; $j = 1, 2, 3, \ldots, n_\Theta$; n_Θ denotes the number of parameters to be estimated. $\delta\Theta_j$ is a small perturbation in the j^{th} parameter. The parameter vector Θ can be updated as follows:

$$\Theta_{k+1} = \Theta_k + \Delta\Theta \tag{20}$$

A flow chart presented in Fig. 2 demonstrates the stepwise procedure of the parameter estimation methodology. The flight testing for the identification of the aircraft is carried out by investigating the longitudinal and lateral-directional modes such as phugoid, short-period, roll, Dutch roll, etc. These modes are excited by applying pulse, step or multistep control commands to elevator, aileron, rudder or throttle setting for the generation of the flight data[36]. A data acquisition unit gathers the aircraft's motion and control variables of the real flight test, and the data is appropriately transformed to the centre of gravity location. Usually, the raw data is corrupted due to the biases, scaling and time synchronisation errors, which are essentially improved by the flight reconstruction technique to ensure the consistency and compatibility of the data[5,6]. The flight experiment is repeated to improve the model fidelity within the specified tolerance limit.

The motion and control variables are appropriately chosen from the compatible flight data set for the non-linear mapping of the specified neural model as shown in Fig. 1. The quantities of the dataset are of different physical significance; hence, they are normalised in a predefined scale level for effective learning of the network. The non-linear mapping is carried out by following the steps discussed in previous section. The tuning parameters of the network are selected such as to achieve the minimum value of the MSE and a higher value of R^2, as close to 1. At the beginning of the optimisation algorithm, the force and moment coefficients of the aerodynamic model are computed using the initial guess values of the parameters (Θ_0) and propagated through the trained network for prediction of the output and perturbed output corresponding to the perturbation in the parameter ($\delta\Theta$), as followed by the Equation (19). In the subsequent steps, the cost function is computed, and the algorithm is checked for the convergence. If the convergence is not met, the aerodynamic parameters are updated by using the GN method as per Equation (20). The iterative process is continued until the convergence is met.

https://doi.org/10.1017/aer.2019.123 Published online by Cambridge University Press

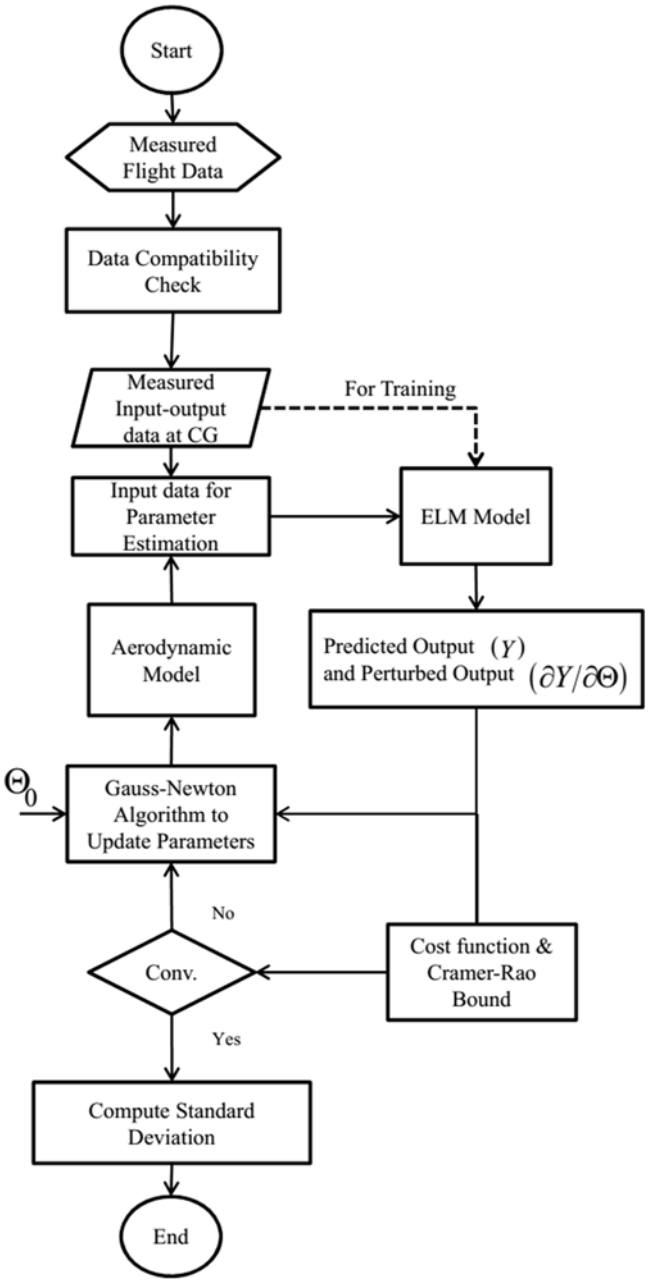

Figure 2. Flow chart of parameter estimation methodology.

Finally, the standard deviations of the optimised parameters are computed by the following expression:

$$\sigma_{\Theta_i} = \sqrt{p_{ii}}, \tag{21}$$

https://doi.org/10.1017/aer.2019.123 Published online by Cambridge University Press

where p_{ii} is the diagonal element of the estimation error covariance matrix, P which is defined as follows:

$$P \approx \left\{ \sum_{i=1}^{N} \left[\frac{\partial Y(i)}{\partial \Theta} \right]^T R^{-1} \left[\frac{\partial Y(i)}{\partial \Theta} \right] \right\}^{-1} \tag{22}$$

4.0 RESULTS AND DISCUSSION

The present section demonstrates the effectiveness of the proposed parameter estimation methodology in the extraction of the stability and control derivatives from the real flight data of Hansa-3 and ATTAS aircrafts.

4.1 Estimation of longitudinal aerodynamics parameters: Hansa-3 aircraft

In the first case study, the longitudinal real flight data (RFD) of the Hansa-3 aircraft were considered[34] and gathered in a calm atmospheric condition by applying a multistep elevator command at a cruise speed of 46m/s and at an altitude of 6,000ft. (approx. 1,829m) as shown in Fig. 3. The raw flight data went through the data compatibility check to improve its quality in terms of biases, scale factors, etc. The flight data contains the motion and control variables, such as α, θ, q, V, a_x, a_z, δ_e etc., whereas the other necessary variables and the coefficients of forces and moments are derived by using the measured quantities and geometrical values[37]. For the modelling of C_D, input variables α and δ_e are considered, whereas α, $q\bar{c}/2V$, δ_e are considered for the modelling of the coefficients C_L and C_m. The aerodynamic model, whose parameters have to be estimated, is expressed as follows:

$$\begin{aligned} C_D &= C_{D_0} + C_{D_\alpha}\alpha + C_{D_{\delta_e}}\delta_e \\ C_L &= C_{L_0} + C_{L_\alpha}\alpha + C_{L_q}(q\,\bar{c}/2V) + C_{L_{\delta_e}}\delta_e \\ C_m &= C_{m_0} + C_{m_\alpha}\alpha + C_{m_q}(q\,\bar{c}/2V) + C_{m_{\delta_e}}\delta_e \end{aligned} \tag{23}$$

The structure of the neural model as shown in Fig. 1 (a) has been used with the log-sigmoid activation function at the HLNs for processing of the data. Table 1 presents the promising values of MSE and R^2 and the number of HLNs achieved in the neural modelling. Figures 4 and 5 show that the estimated quantities from FEM and ELM provide a fairly good match with their respective measured ones. It is to be noted that the estimated responses of FEM are obtained using the integration of the longitudinal equations of motion, whereas ELM responses are obtained through the trained neural model. It is observed that the values of MSE obtained using FEM are 2.84E-02 and 3.53E-02 for RFD01 and RFD02, respectively, which are found to be greater than those obtained using ELM as shown in Table 1. Therefore, Figs. 4 and 5 demonstrate that the quantities based on the ELM network fit better with their measured quantities rather than those of FEM.

The optimisation methodology discussed in the previous section is applied to compute the aerodynamic parameters of the postulated aerodynamic model. The initial values of the stability and control derivatives are chosen closer to the results of EEM. Furthermore, the force and moment coefficients of the aerodynamic model are computed analytically for their propagation through the trained neural models. The optimised parameters are presented in Table 2. The validation of the estimates has been carried out with the results of EEM and FEM.

https://doi.org/10.1017/aer.2019.123 Published online by Cambridge University Press

Table 1
Statistical quantities of the longitudinal neural model

Quantity	RFD01	RFD02
HLN	22	20
MSE	2.54E-02	2.74E-02
R^2	0.9679	0.9873

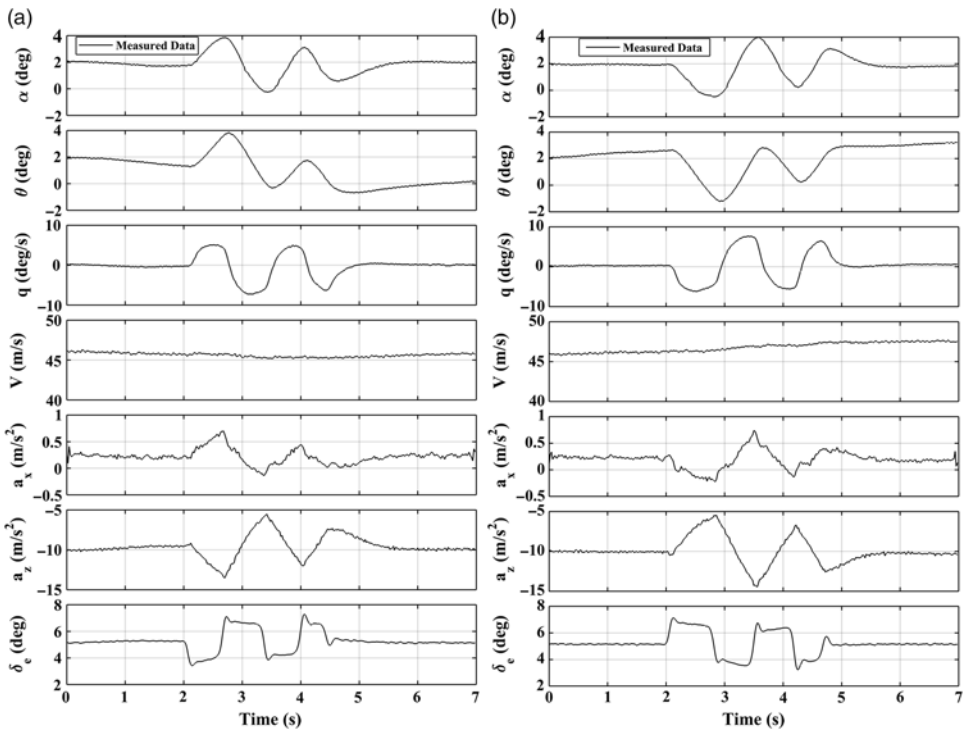

Figure 3. RFD of longitudinal motion: Hansa-3 Aircraft.

EEM, employing the least-square principle, has been applied to estimate the aerodynamic parameters using a linear regression approach[39].

The other conventional method, FEM, has been applied to estimate the parameters with appropriately chosen initial guess values. FEM uses the integration of the dynamic equations of the aircraft while minimising the residual error in an iterative way of optimisation. The method is highly dependent on the integration method, the initial conditions and the initial values of the parameters. Due to the improper selection of the tuning parameters, FEM can require a large number of iterations for convergence of the algorithm or numerically diverge the solution. In Table 2, it is observed that ELM-GN can estimate the aerodynamic parameters closer to the EEM and FEM methods.

Among the estimates, C_{D_0}, C_{L_0}, C_{L_α}, C_{m_α}, $C_{m_{\delta e}}$ can also be validated with the nominal values (NVs) obtained from the wind-tunnel test, whereas the other parameters are found to be

https://doi.org/10.1017/aer.2019.123 Published online by Cambridge University Press

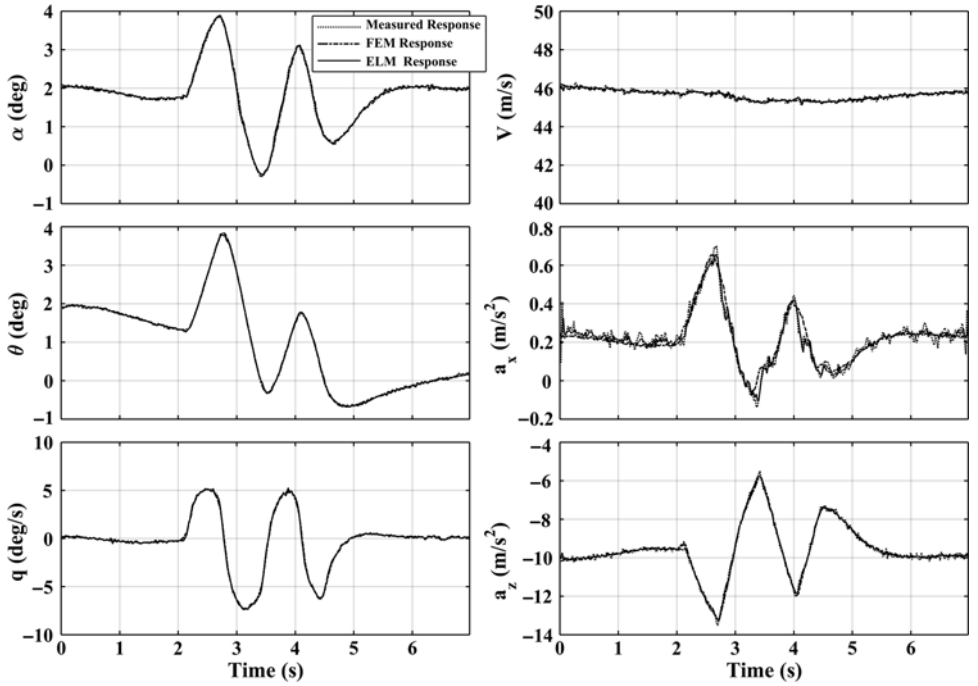

Figure 4. Estimated responses using FEM and ELM: RFD01.

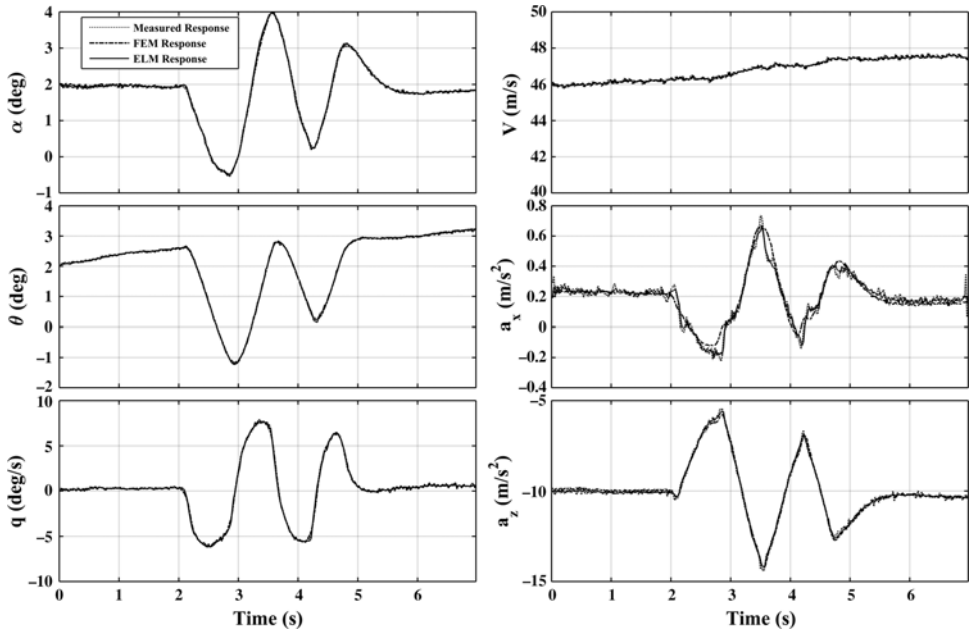

Figure 5. Estimated responses using FEM and ELM: RFD02.

https://doi.org/10.1017/aer.2019.123 Published online by Cambridge University Press

Table 2
Longitudinal parameters of the HANSA-3 aircraft

		RFD01			RFD02		
$\hat{\Theta}$	NV[38]	EEM	FEM	ELM-GN	EEM	FEM	ELM-GN
C_{D_o}	0.035	−0.0349 (0.0009)[#]	0.0349 (0.0010)	0.0363 (0.0008)	0.0361 (0.0010)	0.0362 (0.0010)	0.0380 (0.0008)
C_{D_α}	0.086	0.1827 (0.0094)	0.1797 (0.0097)	0.1841 (0.0083)	0.1598 (0.0091)	0.1595 (0.0092)	0.1755 (0.0083)
$C_{D_{\delta_e}}$	0.026	0.1804 (0.0100)	0.1809 (0.0102)	0.1717 (0.0090)	0.1708 (0.0102)	0.1689 (0.0102)	0.1660 (0.0091)
C_{L_o}	0.354	0.3592 (0.0040)	0.3520 (0.0044)	0.3796 (0.0055)	0.3510 (0.0047)	0.3469 (0.0047)	0.3641 (0.0093)
C_{L_α}	4.978	4.6329 (0.0470)	4.6096 (0.0525)	4.7476 (0.0764)	4.7265 (0.0501)	4.7329 (0.0498)	4.9537 (0.0974)
C_{L_q}	–	26.5029 (1.224)	27.5718 (1.3463)	22.2460 (1.8895)	24.6533 (1.4383)	24.6898 (1.4146)	25.4994 (2.7020)
$C_{L_{\delta_e}}$	0.265	0.5716 (0.0514)	0.6586 (0.0573)	0.3125 (0.0662)	0.5718 (0.0593)	0.6125 (0.0594)	0.5054 (0.1172)
C_{m_o}	0.052	0.1000 (0.0032)	0.1023 (0.0037)	0.1045 (0.0028)	0.0957 (0.0032)	0.0983 (0.0036)	0.1007 (0.0030)
C_{m_α}	−0.496	−0.5308 (0.0379)	−0.4619 (0.0435)	−0.4711 (0.0357)	−0.5126 (0.0335)	−0.4631 (0.0375)	−0.4823 (0.0339)
C_{m_q}	–	−3.7102 (0.9859)	−5.4853 (1.1446)	−4.8506 (0.8662)	−3.6962 (0.9619)	−5.1917 (1.0821)	−4.9060 (0.9045)
$C_{m_{\delta_e}}$	−1.008	−0.8371 (0.0414)	−0.8880 (0.0481)	−0.9070 (0.0360)	−0.8045 (0.0397)	−0.8482 (0.0453)	−0.8690 (0.0376)

Note: [#] Values in the parentheses indicate the sample standard deviation.

comparable with the values of the conventional estimation methods. The values of the parameters C_{D_α}, $C_{D_{\delta e}}$, $C_{L_{\delta e}}$, C_{m_0}, obtained using the estimation methods, are comparable among themselves, although their wind-tunnel values are found to be lower. It is also seen that the estimates obtained through RFD02 are in a close agreement with the parameters obtained through RFD01. As the ELM-GN method computes the estimates like FEM in an iterative way, the convergence of the parameters from their initial values have been presented in Figs. 6, 7, and 8. EEM estimates have been presented as a straight line with their fixed error bars throughout a chosen number of iterations. In the iterative approaches of optimisation, the role of the initial guess values is crucial for their convergence. Hence, the guess values closer to EEM are provided in FEM, and ELM-GN methods. In case of FEM, the convergence of the method has been ensured by keeping the values of a few aerodynamic parameters away from their EEM results, while such a convergence issue is not observed in the case of the ELM-GN method. It is also observed that more iterations are required for optimisation of the parameters using FEM rather than ELM-GN. A similar convergence is seen with the estimates of RFD02 using the FEM and ELM-GN methods.

The validation of the postulated aerodynamic model has also been carried out using the proof-of-match exercise. The estimates obtained through RFD02 has been used to generate

https://doi.org/10.1017/aer.2019.123 Published online by Cambridge University Press

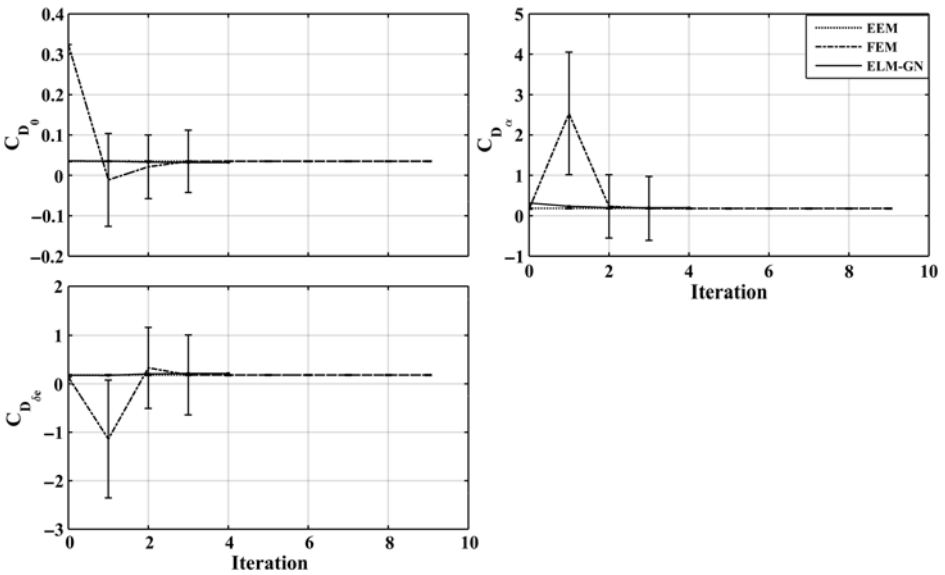

Figure 6. Convergence plot of drag force estimates: RFD01.

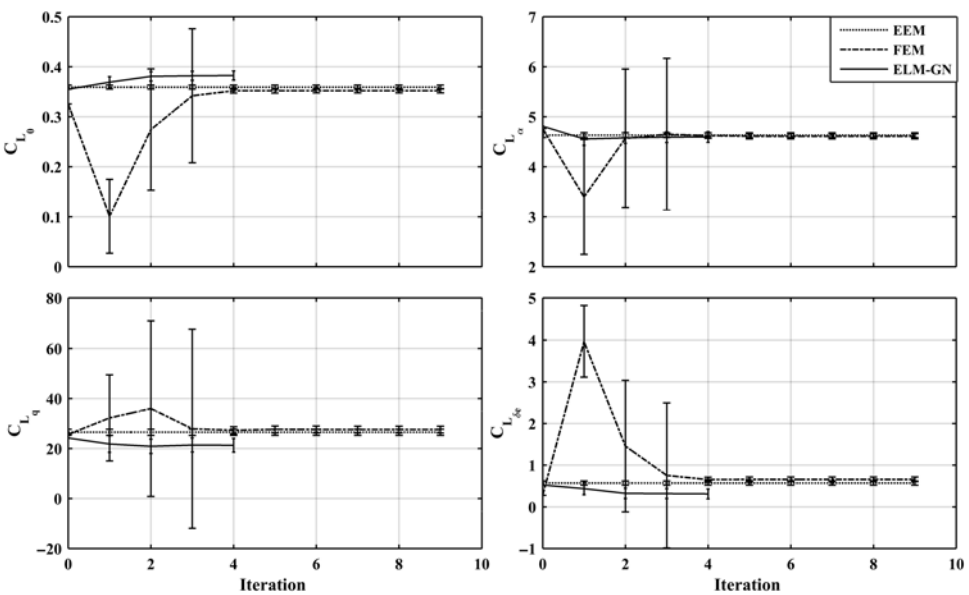

Figure 7. Convergence plot of lift force estimates: RFD01.

the simulated response and compared with the measured response of RFD01 as shown in Fig. 9(a). A similar exercise has also been carried out in the generation of the simulated flight data with the estimates of RFD01 and a doublet elevator command of other real flight data[34], as shown in Fig. 9(b). In both of the figures, it is observed that the simulated responses

https://doi.org/10.1017/aer.2019.123 Published online by Cambridge University Press

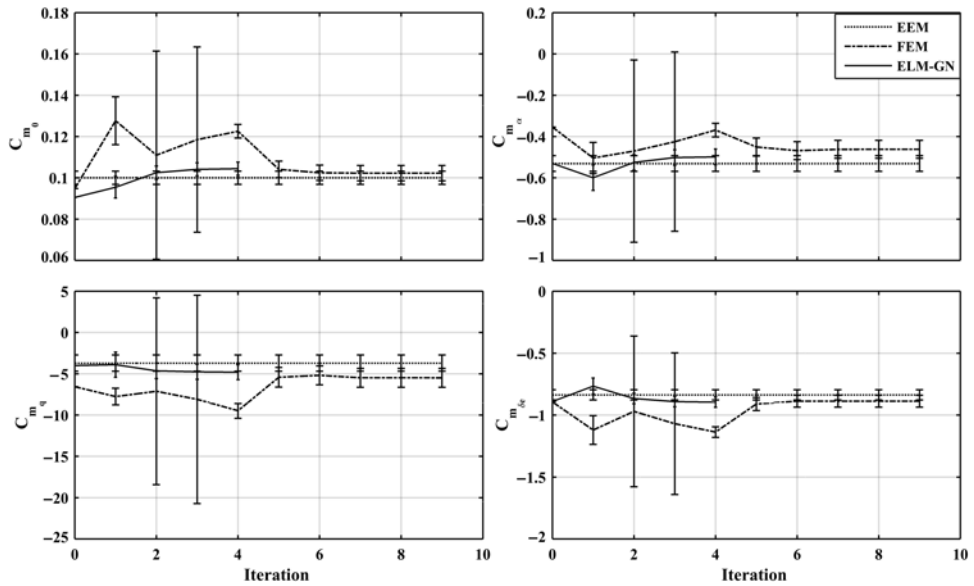

Figure 8. Convergence plot of pitching moment estimates: RFD01.

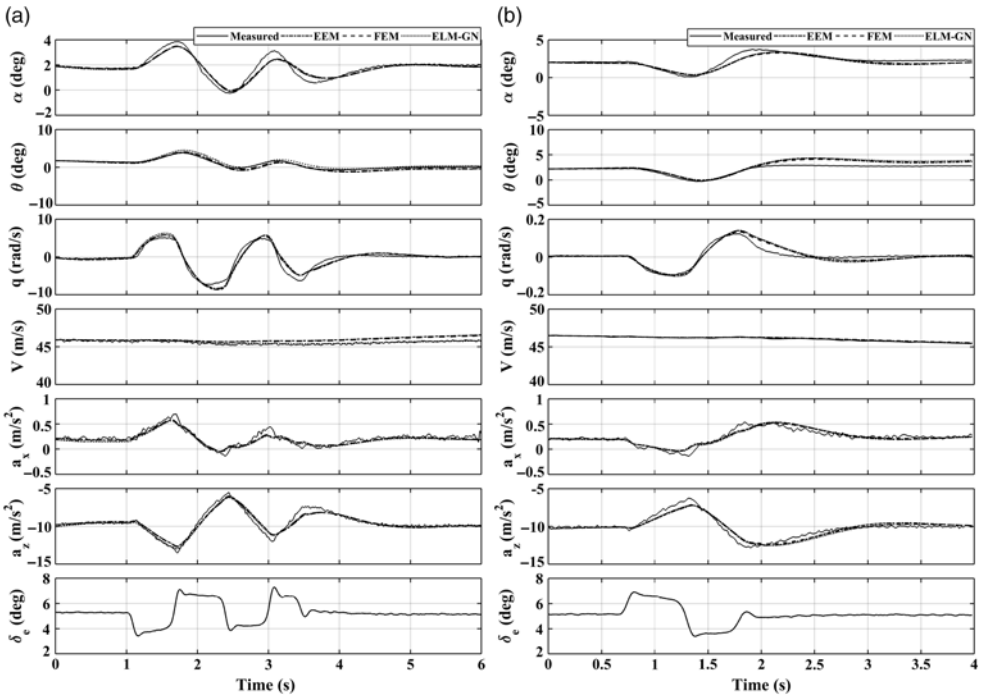

Figure 9. Comparison of measured and simulated flight data using estimates of (a) RFD02 (b) RFD01.

https://doi.org/10.1017/aer.2019.123 Published online by Cambridge University Press

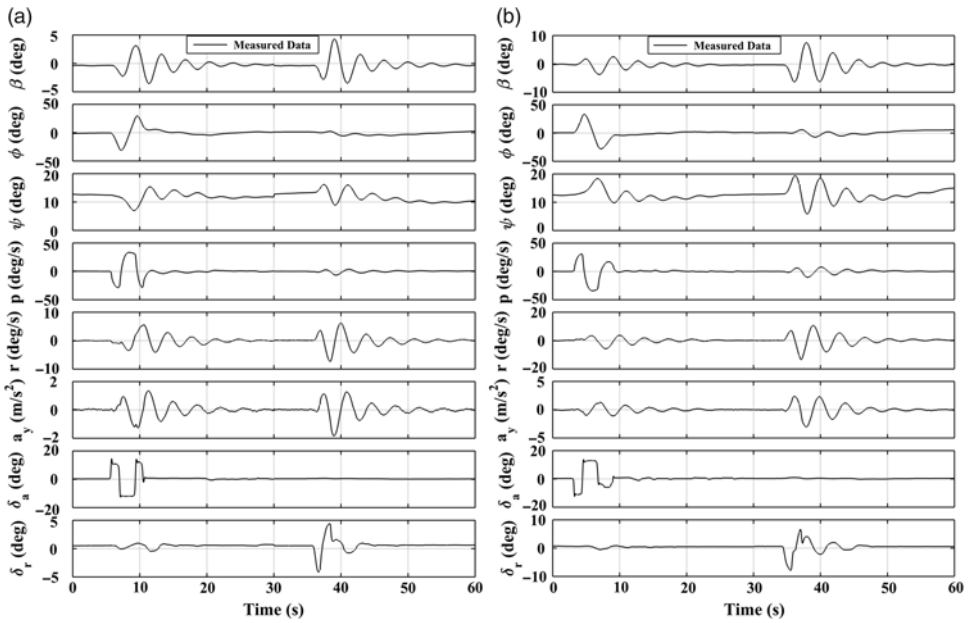

Figure 10. RFD of lateral-directional motion: ATTAS Aircraft.

generated using the estimates of EEM, FEM and ELM-GN are matching satisfactorily with their corresponding measured motion variables of the aircraft.

4.2 Estimation of lateral-directional aerodynamics parameters: ATTAS aircraft

In the second case study, the objective is to extract the aerodynamic stability and control derivatives from the RFD of ATTAS aircraft[5], which was obtained in calm weather at a nominal speed of 200kn (approx. 103m/s) and at an altitude of 16,000ft (approx. 4,877m) as shown in Fig. 10. The data presents a compatible RFD of lateral-directional motion gathered by exciting the roll and Dutch-roll modes using multistep aileron and rudder commands for 30 seconds each, respectively. The data contain the essential motion and control variables, such as β, ϕ, ψ, p, r, δ_a, δ_r, gathered at a sample rate of 0.04 seconds. The aerodynamic force and moment coefficients for postulation of an aerodynamic model are computed from the measured and geometrical quantities[37]. The aerodynamic model, whose parameters must be determined, is expressed as follows:

$$\begin{aligned} C_Y &= C_{Y_0} + C_{Y_\beta}\beta + C_{Y_p}(p\,b/2V) + C_{Y_r}(r\,b/2V) + C_{Y_{\delta_a}}\delta_a + C_{Y_{\delta_r}}\delta_r \\ C_l &= C_{l_0} + C_{l_\beta}\beta + C_{l_p}(p\,b/2V) + C_{l_r}(r\,b/2V) + C_{l_{\delta_a}}\delta_a + C_{l_{\delta_r}}\delta_r \\ C_n &= C_{n_0} + C_{n_\beta}\beta + C_{n_p}(p\,b/2V) + C_{n_r}(r\,b/2V) + C_{n_{\delta_a}}\delta_a + C_{n_{\delta_r}}\delta_r \end{aligned} \tag{24}$$

The aerodynamic model described by Equation (24) presents the dependency of the side-force, rolling and yawing moment coefficients on side-slip angle (β), angular roll and yaw

https://doi.org/10.1017/aer.2019.123 Published online by Cambridge University Press

Table 3
Statistical quantities of the lateral-directional neural model

Quantity	RFD03	RFD04
HLN	30	28
MSE	1.98E-04	2.99E-04
R^2	0.9988	0.9993

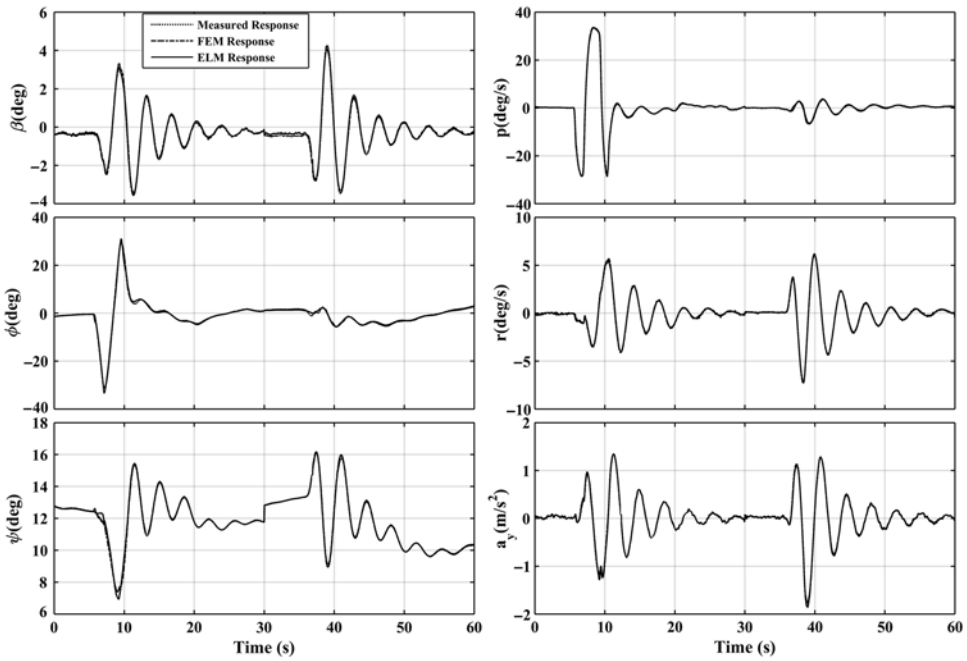

Figure 11. Estimated responses using FEM and ELM: RFD03.

rates (p, r) and control surface deflections of aileron and rudder (δ_a, δ_r), whereas the effects of the other longitudinal variables are neglected. Initially, the flight dynamic neural model (in a restricted sense) for the purpose of aircraft parameter estimation is developed by using the lateral-directional neural model, as shown in Fig. 1 (b). Table 3 presents the statistical values of MSE and R^2 obtained in the neural modelling. It is observed that the value of R^2 is found to be 0.99 with lower values of MSE in both cases, which demonstrate the quality of the neural model for subsequent step in the parameter estimation methodology. Figures 11 and 12 represent the estimated responses of the neural models and FEM obtained through RFD03 and RFD04, respectively. Also, in this case, it is reported that the values of MSE obtained using FEM are found to be higher at 2.20E-04 and 5.61E-04 for RFD03 and RFD04, respectively, in comparison to the values obtained using the ELM network as shown in Table 3. Hence, the quantities modelled using the ELM network fit better in contrast to those of FEM. The coefficients of the aerodynamic model signify the input state/variables of the network, which are

https://doi.org/10.1017/aer.2019.123 Published online by Cambridge University Press

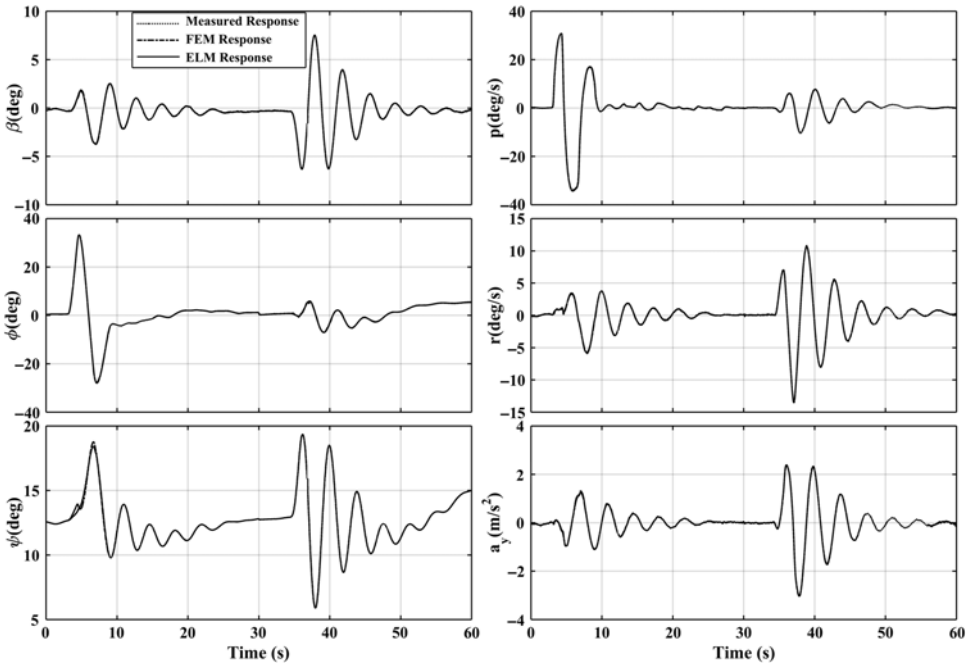

Figure 12. Estimated responses using FEM and ELM: RFD04.

propagated through the trained network for the computation of the aerodynamic parameters. The optimisation algorithm is initialised with the guess values closer to the obtained estimates of EEM, and the optimal estimates are presented in Table 4 for their validation using the estimates of the conventional methods.

From Table 4, it is observed that $C_{Y_0}, C_{Y_{\delta_a}}, C_{l_0}, C_{n_0}, C_{n_{\delta_a}}$ are the weaker derivatives, whereas $C_{Y_\beta}, C_{Y_p}, C_{Y_r}, C_{Y_{\delta_r}}, C_{l_\beta}, C_{l_p}, C_{l_r}, C_{l_{\delta_a}}, C_{l_{\delta_r}}, C_{n_\beta}, C_{n_p}, C_{n_r}, C_{n_{\delta_r}}$ are the strong derivatives in their respective coefficients of the aerodynamic model. It is also observed that the proposed method is capable to estimate the weaker as well as the strong derivatives with the lower standard deviations. The values of the parameters have been found in close agreement with the estimated values of EEM and FEM. Figures 13–15 present the convergence plots of the aerodynamic parameters obtained from FEM and ELM-GN. It is observed that the ELM-GN approach does not report any numerical divergence, whereas FEM reports numerical divergence in the early number of iterations. The size of the error bars represents the standard deviations at each of the iterations. It can also be seen that most of the parameters estimated through the ELM-GN method have converged in the first two iterations, whereas the other iterations have been required due to the sensitivity of the parameters on their respective aerodynamic model coefficients. EEM estimates have been presented with fixed-size error bars as discussed in the earlier subsection. A similar convergence of the estimates is observed through the other flight data RFD03.

Furthermore, the parameters have been validated by the proof-of-match exercise for their simulation-based applications such as the design of flight control laws, flight simulators, etc.

https://doi.org/10.1017/aer.2019.123 Published online by Cambridge University Press

Table 4
Lateral-directional parameter estimates of the ATTAS aircraft

	RFD03			RFD04		
$\hat{\Theta}$	EEM	FEM	ELM-GN	EEM	FEM	ELM-GN
C_{Y_0}	−0.0067	−0.0067	−0.0067	−0.0075	−0.0075	−0.0076
	(5.4E-05)[#]	(4.4E-05)	(5.38E-05)	(4.8E-05)	(3.7E-05)	(5.2E-05)
C_{Y_β}	−1.0508	−1.0552	−1.0447	−1.0339	−1.0351	−1.0309
	(0.0021)	(0.0018)	(0.0020)	(0.0016)	(0.0013)	(0.0016)
C_{Y_p}	0.2093	0.2160	0.2075	0.1599	0.1609	0.1625
	(0.0058)	(0.0047)	(0.0052)	(0.0065)	(0.0050)	(0.0064)
C_{Y_r}	0.6353	0.6430	0.6247	0.6127	0.6174	0.5976
	(0.0161)	(0.0132)	(0.0155)	(0.0111)	(0.0085)	(0.0117)
$C_{Y_{\delta_a}}$	0.0089	0.0103	0.0087	0.0037	0.0037	0.0054
	(0.0011)	(0.0009)	(0.0010)	(0.0013)	(0.0010)	(0.0012)
$C_{Y_{\delta_r}}$	0.1918	0.1930	0.1825	0.1933	0.1944	0.1911
	(0.0034)	(0.0028)	(0.0034)	(0.0024)	(0.0018)	(0.0025)
C_{l_0}	−1.3E-04	6.0E-05	−9.55E-05	−3.0E-05	1.5E-04	−2.0E-05
	(1.2E-05)	(2.6E-05)	(3.92E-05)	(1.1E-05)	(2.3E-05)	(2.9E-05)
C_{l_β}	−0.0561	−0.0614	−0.0561	−0.0585	−0.0646	−0.0551
	(0.0005)	(0.0010)	(0.0013)	(0.0004)	(0.0008)	(0.0008)
C_{l_p}	−0.3785	−0.3888	−0.3666	−0.3931	−0.4022	−0.3766
	(0.0013)	(0.0029)	(0.0040)	(0.0015)	(0.0032)	(0.0036)
C_{l_r}	0.1413	0.1436	0.1272	0.1148	0.1161	0.1088
	(0.0035)	(0.0079)	(0.0107)	(0.0025)	(0.0053)	(0.0056)
$C_{l_{\delta_a}}$	−0.0965	−0.0990	−0.0917	−0.0988	−0.1012	−0.0934
	(0.0002)	(0.0005)	(0.0008)	(0.0003)	(0.0006)	(0.0007)
$C_{l_{\delta_r}}$	0.0217	0.0225	0.0164	0.0205	0.0212	0.0169
	(0.0007)	(0.0017)	(0.0023)	(0.0005)	(0.0011)	(0.0012)
C_{n_0}	0.0014	0.0014	0.0012	0.0014	0.0014	0.0013
	(1.0E-05)	(2.1E-05)	(2.20E-05)	(8.0E-06)	(1.5E-05)	(2.0E-05)
C_{n_β}	0.1290	0.1304	0.1234	0.1314	0.1324	0.1277
	(0.0004)	(0.0008)	(0.0007)	(0.0003)	(0.0005)	(0.0005)
C_{n_p}	−0.0468	−0.0505	−0.0393	−0.0507	−0.0530	−0.0459
	(0.0011)	(0.0024)	(0.0012)	(0.0011)	(0.0021)	(0.0013)
C_{n_r}	−0.0687	−0.0746	−0.0735	−0.0696	−0.0734	−0.0641
	(0.0030)	(0.0063)	(0.0050)	(0.0020)	(0.0035)	(0.0035)
$C_{n_{\delta_a}}$	−0.0060	−0.0064	−0.0054	−0.0069	−0.0073	−0.0060
	(0.0002)	(0.0004)	(0.0002)	(0.0002)	(0.0004)	(0.0003)
$C_{n_{\delta_r}}$	−0.0718	−0.0724	−0.0592	−0.0745	−0.0753	−0.0647
	(0.0006)	(0.0014)	(0.0015)	(0.0004)	(0.0008)	(0.0010)

Note: [#] Values in parentheses indicate the sample standard deviations.

The simulated flight data have been generated by using the estimates of EEM, FEM and ELM-GN, as shown in Figs. 16 and 17. In Fig. 16, the aileron command of RFD04 has been used to generate the simulated data with the estimates of RFD03. In Fig. 17, the rudder command of RFD03 has been used to generate the simulated data with the estimates of RFD04. In both of

https://doi.org/10.1017/aer.2019.123 Published online by Cambridge University Press

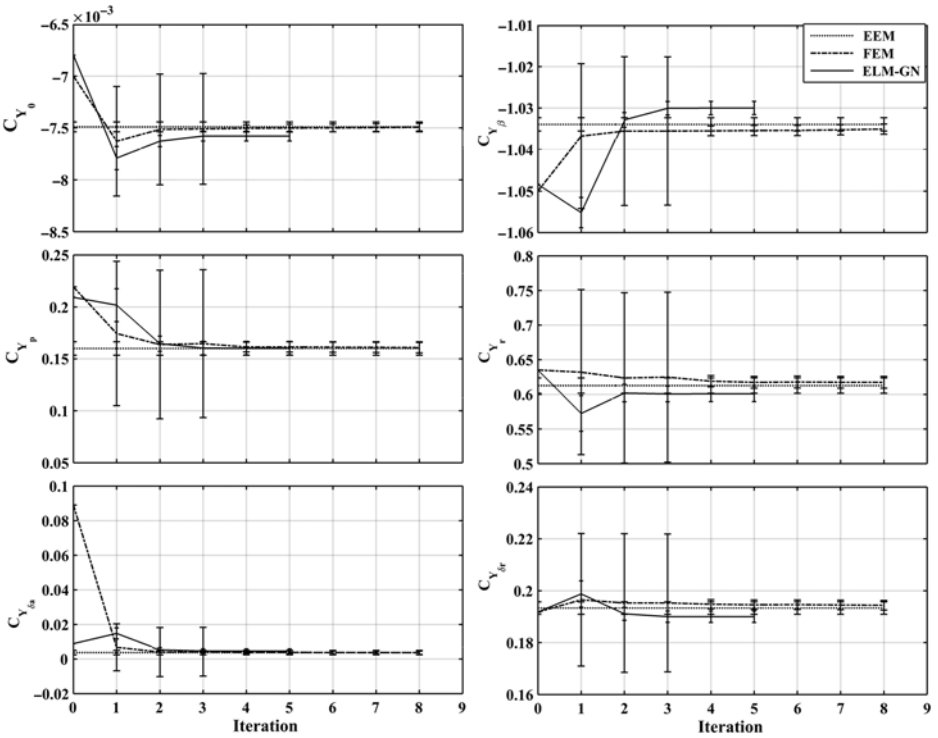

Figure 13. Convergence plot of side force estimates: RFD04.

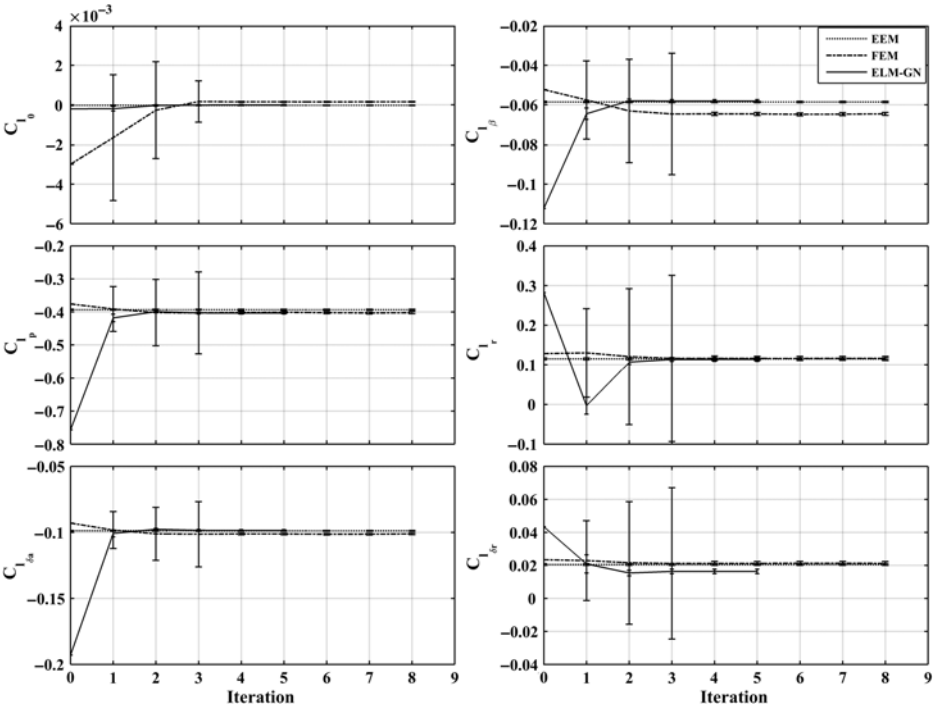

Figure 14. Convergence plot of rolling moment estimates: RFD04.

https://doi.org/10.1017/aer.2019.123 Published online by Cambridge University Press

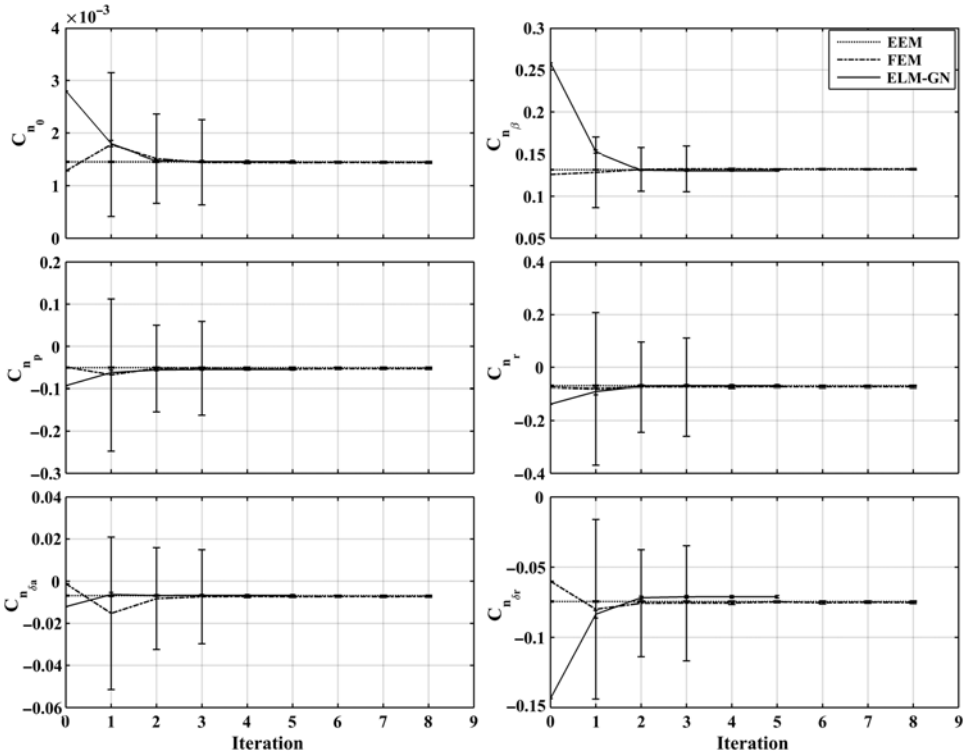

Figure 15. Convergence plot of yawing moment estimates: RFD04.

the figures, it can be observed that most of the simulated quantities match satisfactorily with their respective measured ones.

5.0 CONCLUSION

The parameter estimation methodology, a combined approach of an ELM network with the GN method, has been demonstrated for computation of the aerodynamic parameters from the measured RFD pertaining to the longitudinal as well as the lateral-directional motion. The approach yields good non-linear mapping with satisfactory values of MSE and R^2 between the chosen input and output variables of the ELM network. In the second phase of the algorithm, the investigation of the aerodynamic parameters confirmed that the GN method performed better with the ELM network in terms of computational cost and its convergence. It was noticed that the under-fit as well as the over-fit of the non-linear ELM network may lead to non-optimum estimates in spite of a lower value of MSE; hence, the network size was appropriately determined based on the variables of the input-output space and the number of data samples. The proposed method did not encounter the numerical divergence as reported in the FEM method and converged in a few iterations. The algorithm of FEM was found to be sensitive to the selection of the initial guess values, whereas such issue was not reported with

https://doi.org/10.1017/aer.2019.123 Published online by Cambridge University Press

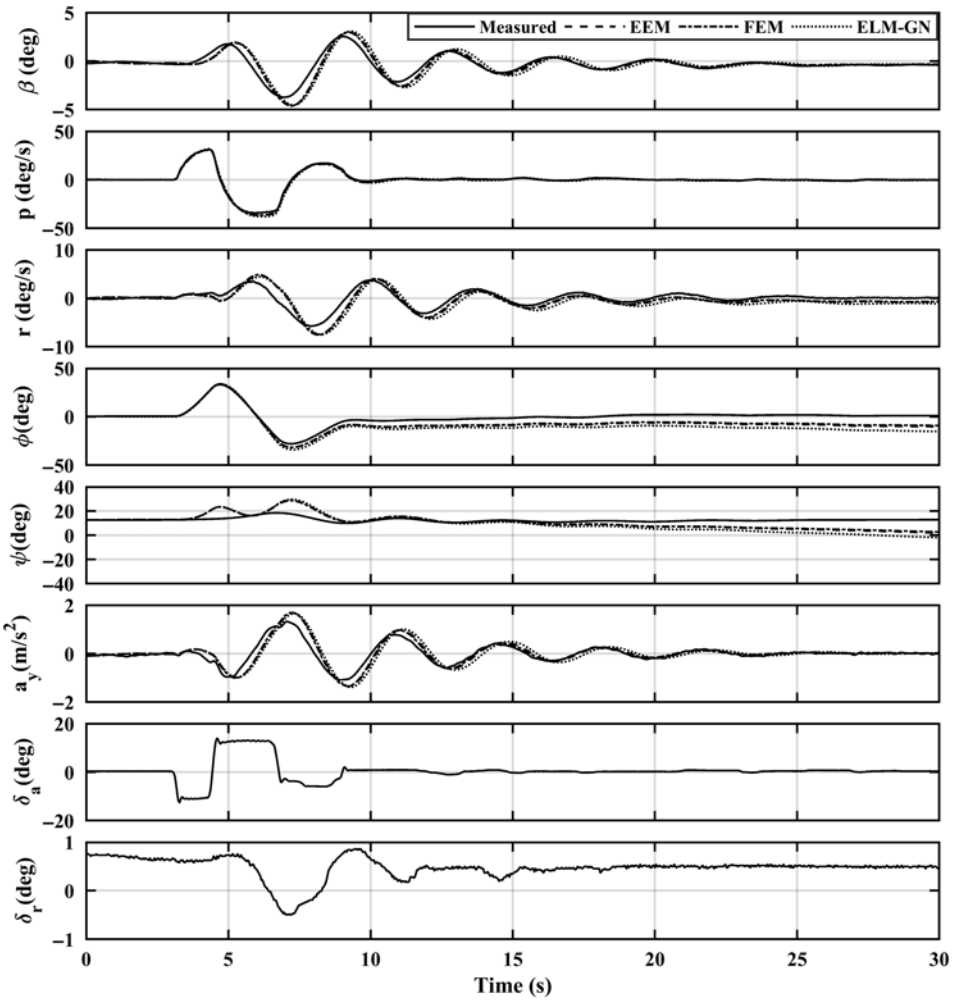

Figure 16. Comparison of measured and simulated flight data using estimates of RFD03.

that of the ELM-GN. The aerodynamic estimates of the longitudinal as well as the lateral-directional motion were estimated in terms of quantity and quality as compared to those of obtained through EEM and FEM. It was also observed that the proposed method was able to estimate the weak as well as the strong derivatives. Finally, the proof-of-match exercise performed on the estimates demonstrated their applications in the field of flight simulation operations. The proposed algorithm neither requires the integration of the equations of the dynamic system nor was found to be sensitive to the initial guess values of the parameters. Moreover, the neural model can capture the flight dynamics of the aircraft at a lower computational cost, and the parameters are optimised along with their corresponding standard deviations in a few iterations. Therefore, the ELM-GN algorithm could be a better alternative to estimate the aerodynamic parameters where the system dynamics are difficult to express due to the non-linearities associated with the unsteady aerodynamics at higher angle-of-attack regions and when a lower value of the computational cost persists.

https://doi.org/10.1017/aer.2019.123 Published online by Cambridge University Press

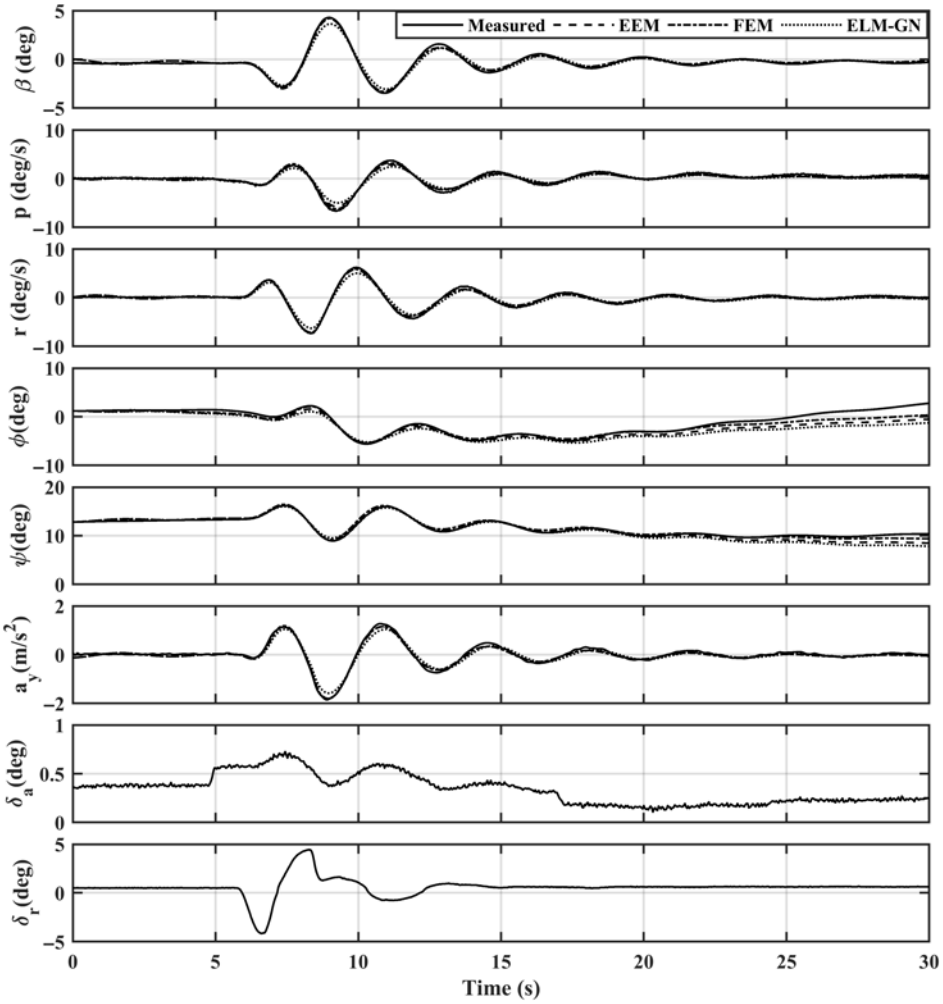

Figure 17. Comparison of measured and simulated flight data using estimates of RFD04.

REFERENCES

1. WASZK, M.R. and SCHMIDT, D.K. Flight dynamics of aero-elastic vehicle, *Journal of Aircraft*, 1988, **25**, (6), pp 563–571. doi:10.2514/3.45623.
2. ETKIN, B. *Dynamic of Flight Stability and Control*, John Wiley and Sons, 1982, New York, US.
3. MAINE, R.E. and ILIFF, K.W. Application of Parameter Estimation to Aircraft Stability and Control – The Output Error Approach. NASA RP 1168, January 1986.
4. RAOL R., JITENDRA G.G. and SINGH J. *Modelling and Parameter Estimation of Dynamic System*, IET, 2004, London, UK.
5. JATEGAONKAR R.V. *Flight Vehicle System Identification: A Time Domain Methodology*, 1st ed, vol. 216, Progress in Astronautics and Aeronautics, AIAA, 2006, Reston, VA, US. doi:10.2514/4.866852.
6. KLEIN, V. and MORELLI, E. *Aircraft System Identification: Theory and Practice, AIAA Education Series*, AIAA, 2006, Reston, VA, US.

https://doi.org/10.1017/aer.2019.123 Published online by Cambridge University Press

7. JATEGAONKAR R.V. and PLAETSCHKE E. Identification of moderately nonlinear flight mechanics systems with additive process and measurement noise, *Journal of Guidance, Control, and Dynamics*, 1990, **13**, (2), pp 277–285. doi:10.2514/3.20547.
8. CHOWDHARY G. and JATEGAONKAR R.V. Aerodynamic parameter estimation from flight data applying extended and unscented Kalman filter, AIAA Atmospheric Flight Mechanics Conference, Keystone, CO, US, 2006. doi:10.2514/6.2006-6146.
9. HORNIK K. Approximation capabilities of multilayer feed-forward networks, *Neural Network*, 1991, **4**, (2), pp 251–257. doi:10.1016/0893-6080(91)90009-T.
10. RUMELHART D.E. HINTON G.E. and WILLIAMS R.J., Learning representations by back propagation errors, *Nature*, 1986, **323**, pp 533–536. doi:10.1038/323533a0.
11. HAYKIN S. *Neural Networks and Learning Machines*, 3rd ed, Prentice-Hall, 2009, Englewood Cliffs, NJ, US.
12. PRATIHAR D.K. *Soft Computing: Fundamentals and Applications*, Narosa Publishing House, 2008, New Delhi, India.
13. LINSE D.J. and STENGEL R. Identification of aerodynamic coefficients using computational neural networks, *Journal of Guidance, Control, and Dynamics*, 1993, **16**, (6), pp 1018–1025. doi:10.2514/3.21122.
14. RAISINGHANI S.C., GHOSH A.K. and KALRA P.K. Two new techniques for aircraft parameter estimation using neural networks, *Aeronautical Journal*, 1998, **102**, (1011), pp 25–30. doi:10.1017/S0001924000065702.
15. SINGH S. and GHOSH A.K. Estimation of lateral-directional parameters using neural network based modified delta method, *Aeronautical Journal*, 2007, **111**, (1124), pp 659–667. doi:10.1017/S0001924000004838.
16. GARHWAL R., HALDER A. and SINHA M. Sensitivity analysis using neural network for estimating aircraft stability and control derivatives, IEEE International Conference on Intelligent and Advanced Systems, Kuala Lumpur, Malaysia, 2007. doi:10.1109/ICIAS.2007.4658380.
17. DAS S., KUTTERI R.A., SINHA M. and JATEGAONKAR R.V. Neural partial differential method for extracting aerodynamic derivatives from flight data, *Journal of Guidance, Control, and Dynamics*, 2010, **33**, (2), pp 376–384. doi:10.2514/1.46053.
18. PEYADA N.K. and GHOSH A.K. Aircraft parameter estimation using new filtering technique based on neural network and Gauss-Newton method, *Aeronautical Journal*, 2009, **113**, (1142), pp 243–252. doi:10.1017/S0001924000002918.
19. KUMAR R. and GHOSH A.K. Nonlinear longitudinal aerodynamic modeling using neural Gauss-Newton method, *Journal of Aircraft*, 2011, **48**, (5), pp 1809–1812. doi:10.2514/1.C031253.
20. SADERLA S., DHAYALAN R. and GHOSH A.K. Non-linear aerodynamic modelling of unmanned cropped delta configuration from experimental data, *Aeronautical Journal*, 2017, **121**, (1237), pp 320–340. doi:10.1017/aer.2016.124.
21. KUMAR R., GANGULI R., OMKAR S.N. and KUMAR M.V. Rotorcraft parameter identification from real time flight data, *Journal of Aircraft*, 2008, **45**, (1), pp 333–341. doi:10.2514/1.32024.
22. SANWALE J. and SINGH D.J. Aerodynamic parameters estimation using radial basis function neural partial differentiation method, *Defence Science Journal*, 2018; **68**, (3), pp 241–250. doi:10.14429/dsj.68.11843.
23. KUMAR A. and GHOSH A.K. ANFIS-delta method for aerodynamic parameter estimation using flight data, *Journal of Aerospace Engineering*, 2019, **233**, (8), pp 3016–3032. doi:10.1177/0954410018791621.
24. ROY A.G. and PEYADA N.K. Aircraft parameter estimation using hybrid neuro fuzzy and artificial bee colony optimization (HNFABC) algorithm, *Journal of Aerospace Science and Technology*, 2017, **71**, pp 772–782. doi:10.1016/j.ast.2017.10.030.
25. HUANG G.B., ZHU Q.Y. and SIEW C.K. Extreme learning machine: a new learning scheme of feed forward neural networks, IEEE International Joint Conference on Neural Networks, 2004, Budapest, Hungary. doi:10.1109/IJCNN.2004.1380068.
26. HUANG G.B., ZHU Q.Y. and SIEW C.K. Extreme learning machine: theory and applications, *Neurocomputing*, 2006, **70**, (1–3), pp 489–501. doi:10.1016/j.neucom.2005.12.126.
27. SUN, Z.L., CHOI, T.M., AU, K.F. and YU Y. Sales forecasting using extreme learning machine with applications in fashion retailing, *Decision Support Systems*, 2008, **46**, (1), pp 411–419. doi:10.101 6/j.dss.2008.07.009.

28. CHACKO, B.P., KRISHNAN, V.R.V., RAJU, G. and ANTO, P.B. Handwritten character recognition using wavelet energy and extreme learning machine, *International Journal of Machine Learning and Cybernetics*, 2012, **3**, (2), pp 149–161. doi:10.1007/s13042-010049-5.
29. ZHAO Z., LI P. and XU X. Forecasting model of coal mine water inrush based on extreme learning machine, *Applied Mathematics and Information Sciences*, 2013, **7**, (3), pp 1243–1250. doi:10.12785/amis/070349.
30. PAL M. Extreme learning machine-based land cover classification, *International Journal of Remote Sensing*, 2009, **30**, (14), pp 3835–3841. doi:10.1080/01431160902788636.
31. ZONG W.W. and HUANG G.B. Face recognition based on extreme learning machine, *Neurocomputing*, 2011, **74**, (16), pp 2541–2551. doi:10.1016/j.neucom.2010.12.041.
32. PAMADI B.N. Performance, Stability, Dynamics and Control of Airplanes, AIAA Education Series, 1998, Virginia.
33. SOLA J. and SEVILLA J. Importance of input data normalization for the application of neural networks to complex industrial problems, *IEEE Transactions on Nuclear Science*, 1997, **44**, (3), pp 1464–1468. doi:10.1109/23.589532.
34. PEYADA N.K. Parameter Estimation from Flight Data Using Feed Forward Neural Networks. PhD Thesis, IIT Kanpur, India, 2009.
35. SAHIN M. Comparison of modelling ANN and ELM to estimate solar radiation over Turkey using NOAA satellite data, *International Journal of Remote Sensing*, 2013, **34**, (21), pp 7508–7533. doi:10.1080/01431161.2013.822597.
36. FILIPPONE A. *Flight Performance of Fixed and Rotary Wing Aircraft*, Elsevier, 2006, Oxford, UK.
37. VERMA, H.O., PEYADA N.K. Parameter estimation of stable and unstable aircraft using extreme learning machine, AIAA Atmospheric Flight Mechanics Conference 2018. doi:10.2514/6.2018-0526.
38. RANGARANJAN R. and VISHWANATHAN S. Wind Tunnel Test Results on a 1/5 Scale HANSA Model. NAL TR-01 1997.
39. MORELLI E.A. Practical aspects of the equation error method for aircraft parameter estimation, AIAA Atmospheric Flight Mechanics Conference, Keystone, CO, US, 2006. doi:10.2514/6.2006-6144.

https://doi.org/10.1017/aer.2019.123 Published online by Cambridge University Press